THE JOURNAL OF PHYSICAL CHEMISTRY C
A JOURNAL OF THE AMERICAN CHEMICAL SOCIETY

pubs.acs.org/JPCC

Article

Effect of Wet and Dry Environments in CNC/MWCNTs/Ag_2O Electrically Conductive Films: Material Characterization and Molecular Dynamics Simulation

Francesca Luzi,[#] Ainhoa Angulo Dehesa,[#] Emiliano Laudadio, Debora Puglia, Erlantz Lizundia, Pierluigi Stipa, Ilaria Armentano,[*] and Luigi Torre

Cite This: https://doi.org/10.1021/acs.jpcc.3c04767

Read Online

ACCESS | Metrics & More | Article Recommendations | Supporting Information

ABSTRACT: Electrically conducting biobased materials present a bright future for high-technological applications including sensors, soft electronics, and active packaging. Accordingly, here, we develop and characterize ternary nanohybrid films combining cellulose nanocrystals (CNC), multiwalled carbon nanotubes (MWCNTs) and silver oxide (Ag_2O) nanoparticles. An evaporation-induced self-assembly process is applied to obtain homogeneously dispersed free-standing nanocomposite films as proven by electron microscopy. Thermogravimetric analyses show that MWCNTs delay the cleavage of glycosidic linkages of cellulose, while Ag_2O catalyzed thermodegradation events rendering reduced thermal stabilities. The electrical and dielectrical properties are analyzed under completely dry and 53% humidity atmospheres, and the results are observed also in light of the electric modulus. Water increases the conductivity of binary and ternary systems and shifts the electric modulus relaxation peak. Finally, full atom molecular dynamics (MD) simulations are performed to describe the phenomena on interfaces between nanoscale systems, underlying mechanisms for the obtained electrical AC and DC results. Computational results reveal changes in the CNC/MWCNT/Ag_2O interactions depending on the water content. The combination of experimental and simulation data shown sheds light on the electric conducting mechanism of nanocellulose-based materials with multifunctional properties.

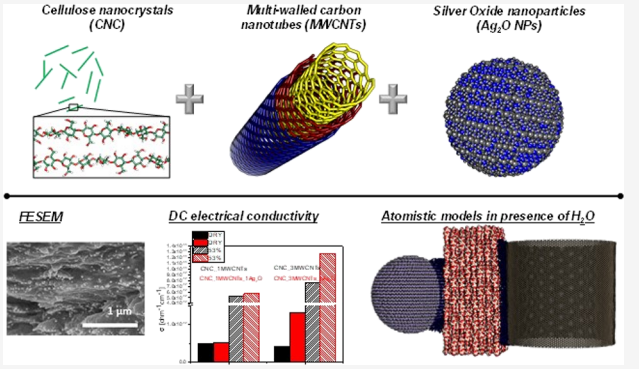

1. INTRODUCTION

The design and development of innovative materials derived from natural sources is currently at the forefront of academic and industrial research.[1−4] Cellulose is the most abundant polysaccharide on Earth and holds a crucial position in abundant organic raw materials, since it is considered as a virtually inexhaustible source of feedstock, meeting the increasing demand for green and biocompatible products.[5]

Cellulose nanocrystals (CNC) are nanoscale biobased materials that can be extracted from a variety of renewable cellulose-rich sources.[6] They are "rod-like" nanoparticles with crystallinity degrees ranging from 80 to 95% and large specific surface areas, which are also combined with unique structural and physicochemical properties.[7] The hybridization of CNC with further nanomaterials permits to develop innovative and multifunctional biobased nanocomposites[8] and efficient and sustainable devices for advanced applications with green properties[9] in film and in 3D structure.[10,11] CNC is intrinsically insulating; however, it is a promising sustainable material for the preparation of conductive nanohybrid materials. CNC can be transformed into one that possesses electrically conductive properties by utilizing various modification strategies that harness their exceptional characteristics.[12−14] In particular, they can be applied as electric heaters, supercapacitors,[13] and sensors,[14] when combined with conductive nanofillers,[15,16] as shielding materials for excellent electromagnetic interference[17] and as parts of electronics and communication devices.[5]

In this research, to attain high-performance conductive and free-standing films, CNCs were combined with multiwalled carbon nanotubes (MWCNTs), to transfer electrical transport properties to the insulating CNC, and with silver oxide nanoparticles (Ag_2O NPs), resulting in conductive cellulose-based films and in electromagnetic nanocomposite materials.[18,19] This work follows a previous study from our group, where we demonstrated that the dispersion of silver oxide

Received: July 15, 2023
Revised: September 28, 2023

Table 1. Binary and Ternary Nanohybrid Film Formulations

samples	CNC	CNC_ 0.5MWCNTs	CNC_ 1MWCNTs	CNC_ 3MWCNTs	CNC_ 4MWCNTs	CNC_ 5MWCNTs	CNC_ 1 Ag_2O	CNC_ 1MWCNTs_ 1 Ag_2O	CNC_ 3MWCNTs_ 1 Ag_2O	CNC_ 5MWCNTs_1 Ag_2O
CNC (wt %)	100	99.5	99.0	97.0	96.0	95.0	99.0	98.0	96.0	94.0
MWCNTs (wt %)		0.5	1.0	3.0	4.0	5.0		1.0	3.0	5.0
Ag_2O NPs (wt %)							1.0	1.0	1.0	1.0

nanoparticles at 1 wt % content in CNC based systems imparts an effective antimicrobial activity to the composite films, killing both *Escherichia coli* RB (*E. coli* RB) and *Staphylococcus aureus* 8325−4 (*S. aureus* 8325−4).[8] In spite of the research works carried out so far to exploit nanocellulose/Ag_2O hybrids into diverse applications including adsorbent for water contaminants,[20] antimicrobial food packaging,[21] or reusable catalysts,[22] the nature of the water-nanocellulose, water-nanosilver or nanocellulose-nanosilver interactions in the presence of water remain practically unexplored. Additionally, the synergy between CNC and MWCNTs promotes high electrical conductivity and interfacial polarization in the electromagnetic fields. Various studies are focused on the electrical conductivity of CNC/MWCNT-based materials;[23] however, systematic analysis of the electrical transport properties of these innovative materials is required to elucidate the interphase properties and the effect of additional nanoparticles in ternary systems.

MWCNTs are carbon nanostructures formed by rolling-up graphene sheets in a cylindrical way; since the discovery of MWCNTs by Ijima,[24] composites filled with MWCNTs have been widely investigated to achieve superior electrical, thermal, and mechanical properties.[25] According to the distribution, disentanglement, and interaction of MWCNTs in polymer chains, nanocomposites with modulated, innovative, and superior properties can be obtained.[5] The role of interface in CNC/MWCNTs nanocomposites has been underlined, even if the mechanism of this interaction is still not fairly elucidated. In this aspect, impedance spectroscopy can be a valuable method to elucidate the mechanism and analyze how the interphase extensively affects the electrical conductivity of MWCNT nanocomposites. The electrical characteristics are related to the volume fraction of the conductive filler, the nanoparticle size, and shape and also to other factors, such as adhesion between the host phase and the matrix, processing methods, and possible interactions between the conductive phase.[25]

The present work is an extension of our previous studies,[8] concerning the physicochemical and electrical/dielectrical properties of two different types of binary systems based on CNC combined with single walled carbon nanotubes[9] or silver nanoparticles.[8] Here, we also analyzed the dependence of electrical transport properties on the synergistic interaction between MWCNTs and Ag_2O NPs, in dry and in wet conditions. The effect of humidity on the electrical conductivity of nanostructured materials have been investigated with the purpose of developing reliable water vapor sensors.

With the aim to identify the interface interactions between MWCNTs and Ag_2O NPs among CNC, molecular dynamics (MD) simulations were carried out. The computational approach is helpful in the exploitation of all short- and long-range phenomena that occur in disperse phases and between different materials. MD simulation acts as a bridge between the macroscopic experimental phenomena and microscopic field, and different studies have already revealed the capabilities of this approach. Li et al.[26] used a combined computational−experimental approach to investigate the adsorption of xanthate from aqueous solution by multilayer graphene oxide. In this work, the MD simulation revealed that the adsorption of xanthate is a spontaneous endothermic process.[26] In another study, MD simulations have been used to investigate the stability of different systems of 3,5-difluoro-2,4,6-trinitroanisole, and 2,4,6,8,10,12-hexanitrohexaazaiso-wurtzitane to design a new melt-cast explosive. In this study, Hu et al. calculated the relatively excellent mass ratio parameter using the MD simulations, and then, they fabricated the theorized systems.[27] Despite this, although there are different works in the literature where MD simulations are combined with experimental approaches, according to the authors' knowledge, this is the first time that these types of systems treated in this work have been investigated using such an approach. In this concern, four different atomistic systems have been modeled: neat CNC, CNC/MWCNTs, CNC/Ag_2O, and CNC/MWCNTs/Ag_2O hybrid materials. MD simulations have also been exploited to provide structural insights into the amount of adsorbed water molecules in the humidity conditions, helping to shed light on the role of water in the modulation of electrical properties of these nanomaterials.

2. EXPERIMENTAL SECTION

2.1. Materials. Multiwalled carbon nanotubes, with a purity of 90% and an outer mean diameter of 10−15 nm were supplied by Arkema (Graphistrength C100). Silver oxide nanoparticles P203, with a size distribution ranging from 20 to 80 nm, were purchased from Cima NanoTech (Corporate Headquarters Saint Paul, MN, USA). Microcrystalline cellulose with a particle size of 20 μm (310697−500G), sulfuric acid, sodium dodecyl sulfate (minimum 98.5%, GC), silica gel (SiO_2), magnesium nitrate-6-hydrate ($Mg(NO_3)_2$), and sodium chloride (NaCl) have been supplied by Sigma-Aldrich. Cellulose nanocrystals (CNC) were synthesized as previously described via sulfuric acid hydrolysis of microcrystalline cellulose (64% sulfuric acid solution at 45 °C for 30 min).[28,29]

2.2. Nanohybrid film processing. MWCNT-based CNC nanohybrid films were developed by evaporation-induced self-assembly (EISA). The required amounts of MWCNTs were finely dispersed in distilled water (in 1 mg1 mL^{-1} concentration) via tip-sonication (30% output for 30 min; Vibra-CellTM CV 334), and they were added to aqueous CNC (2 wt %) dispersions to obtain 0.5, 1.0, 3.0, 4.0, and 5.0 wt % (MWCNT concentration into CNCs, respectively). Then, another sonication step (5 min and 20% output Vibra-CellTM CV 334) and stirring step (30 min, in the case of 3.0, 4.0, and 5.0 wt % films, under a flow of air and hot plate at 100

https://doi.org/10.1021/acs.jpcc.3c04767
J. Phys. Chem. C XXXX, XXX, XXX−XXX

°C were applied to evaporate the excess of water) have been applied to dispersions before casting them onto Teflon dishes. In order to study the synergic interaction between Ag_2O NPs and MWCNTs in CNC-based films, ternary nanohybrids were developed by following a similar procedure. Briefly, MWCNTs were dispersed in distilled water (1 mg1 mL^{-1}) via sonication (30% output for 30 min) to obtain 1.0, 3.0, and 5.0 wt % concentrations. Then, Ag_2O nanoparticles were added in MWCNT solution by tip sonication (20% output for 5 min) and added to 2 wt % aqueous CNC dispersions. Finally, another sonication step at 20% output for a further 5 min was applied to aqueous CNC/MWCNTs/Ag_2O dispersions before casting them. The composition of the developed films is reported in Table 1, where CNC_0.5MWCNTs, CNC_1MWCNTs, CNC_3MWCNTs, and CNC_5MWCNTs specify binary nanohybrid films based on cellulose nanocrystals and 0.5, 1.0, 3.0, and 5.0 wt % of MWCNTs dispersed and CNC_1 Ag_2O indicates binary nanohybrid films based on cellulose nanocrystals and 1 wt % of silver nanoparticles, while CNC_1MWCNTs_1 Ag_2O, CNC_3MWCNTs_1 Ag_2O, and CNC_5MWCNTs_1 Ag_2O specify ternary nanohybrid films based on cellulose nanocrystals, 1.0 wt % of silver nanoparticles, and 1.0, 3.0, or 5.0 wt % of MWCNTs, respectively.

2.3. Nanohybrid Film Characterization. The morphology of CNC-based films was investigated using a Hitachi S-4800 field emission scanning electron microscopy (FE-SEM) instrument at an acceleration voltage of 5 kV. Before characterization, cryogenically fractured surfaces were gold-coated with a 10 nm thick layer using an Emitech K550X sputter coater.

Thermogravimetric analysis (TGA) was performed on 10 mg samples by a Seiko Exstar 6300 TGA quartz rod microbalance. The tests were done under a nitrogen atmosphere from 25 to 900 °C at 10 °C min^{-1}.

Fourier Transform Infrared Spectroscopy (FT-IR) spectra of CNC and CNC binary and ternary nanocomposite films were obtained at room temperature in reflection mode by attenuated total reflectance (ATR) by using a JASCO FT-IR 615 spectrometer with 4 cm^{-1} spectral resolution. Room temperature X-ray powder diffraction (XRD) patterns were obtained in a Bruker D8 Advance diffractometer equipped with a Cu tube, Ge(111) incident beam monochromator (λ = 1.5406 Å) (fixed slit 1 mm), and a Sol-X energy dispersive detector (fixed slit 0.06 mm). Samples were mounted onto a zero-background silicon wafer embedded in a generic sample holder. Bulk electrical resistivity measurements were conducted (ASTM D-257) by using a Keithley 6517A electrometer, by applying a square wave ranging from 25 V (for pure CNC) to 0.1 V (for percolated nanohybrids) with a period of 120 s, of at least four measurements for each sample. The real and imaginary parts of the complex impedance (Z^*) of the CNC and CNC based MWCNTs EISA films were analyzed by Hewlett-Packard 4284A Precision LCR Meter, in the 20 Hz−1 MHz frequency range. The specific AC conductivity of the samples as a function of frequency $\sigma(\omega)$ is calculated as

$$\sigma_{AC} = d/(|Z| \times A) \quad (1)$$

where A is the cross-sectional area and d is sample thickness measured using a Borletti MELN/1W micrometer. Since cellulose is highly sensitive to humidity, films were kept in desiccators with different saturated salts for several days before each measurement in order to stabilize them at a given relative humidity (RH). The following compounds were used: silica gel (SiO_2, RH = 0%) and magnesium nitrate-6-hydrate over saturated solution, $Mg(NO_3)_2$ (RH = 53%).

2.4. Molecular Dynamics (MD) Simulations. Molecular dynamics (MD) simulations have been used to study the interface interactions between neat CNC, MWCNTs, and Ag_2O nanoparticles. As previously mentioned, four different atomistic systems have been prepared: CNC, CNC/MWCNTs, CNC/Ag_2O, and CNC/MWCNTs/Ag_2O nanohybrid.

The starting CNC has been modeled using 64 cellulose chains, each composed of 30 glucan units. Globally, an amount of 1920 units constitutes a CNC, with 16732 atoms. The final dimension of this system was 10 nm in diameter and 18 nm of length. One MWCNT has been also modeled considering a diameter of 13.6 nm and a length of 24.2 nm, with 40800 atoms. About the Ag_2O NPs, a system composed by 92295 atoms with a diameter of 27 nm has been prepared. The four different systems have been modeled considering these three structural files together in the same simulation box following the system type. This means that with the aim to perform reliable MD simulations, the settled boxes were different between them, and they depended on the number of the different models present. For these reasons, the size of the simulation box for CNC was 17.8 nm^3, while a box of 17.8 × 35.6 × 17.8 nm has been settled for the CNC/MWCNTs, CNC/Ag_2O, and CNC/MWCNTs/Ag_2O systems.

To investigate and clarify the role of water on the electrical properties of these systems, water molecules have been randomly included in the simulation box of each system; this means that a total of 8 models have been built, 4 without water, and other four with H_2O molecules. To perform simulations reproducing the real conditions, a relative humidity rate (RH) of 50% has been considering including the half of the total number of molecules that a system could contain. Since this number is strictly correlated to the dimension of the box and the size and the number of systems, to reproduce the same HR, 60,208, 60,811, 77,163, and 78,350, water molecules have been added in CNC, CNC/MWCNTs, CNC/Ag_2O, and CNC/MWCNTs/Ag_2O systems, respectively.

All MD simulations have been performed using GROMACS 5.0.4 suite[30] and CHARMM36 force field[31] with specific parameter extensions to provide an accurate description of nanorod, nanoparticles, and polymer chains and to appropriately predict the effect of the solvent. Systems have been minimized applying periodic box conditions (PBC) in all directions, using a neighbor searching grid type; the cutoff distance for the short-range neighbor list was set to 1.4 nm. Electrostatic interactions have been included by implementing a fast smooth particle-mesh Ewald algorithm[32,33] with 1.4 nm distance for the Coulomb cutoff, which is considered the method of choice to obtain an accurate evaluation of long-range electrostatic interactions in large macromolecular systems.[34,35]

Each system has been subjected to two minimization steps using steepest descent and conjugate gradient algorithms[36] and subsequent six preliminary equilibration steps based on 5 ns of annealing simulations to gradually reach the simulation temperature of 25 °C and generate atomistic velocities. A weak temperature coupling (Berendsen thermostat) with a time constant of 1 ps has been applied to maintain the reference temperature (25 °C) throughout the whole run. The subsequent production step consisted in 100 ns of MD

https://doi.org/10.1021/acs.jpcc.3c04767
J. Phys. Chem. C XXXX, XXX, XXX−XXX

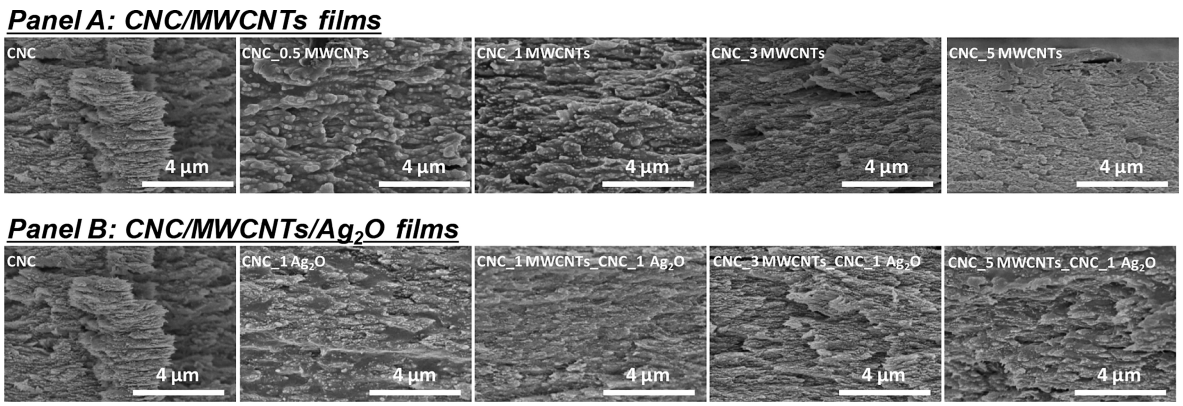

Figure 1. FE-SEM images depicting the fracture cross-section of binary CNC/MWCNTs (A) and ternary CNC/MWCNT/Ag_2O composite films with a varying multiwall carbon nanotube concentration up to 5 wt % (B) (magnification = 12.000×).

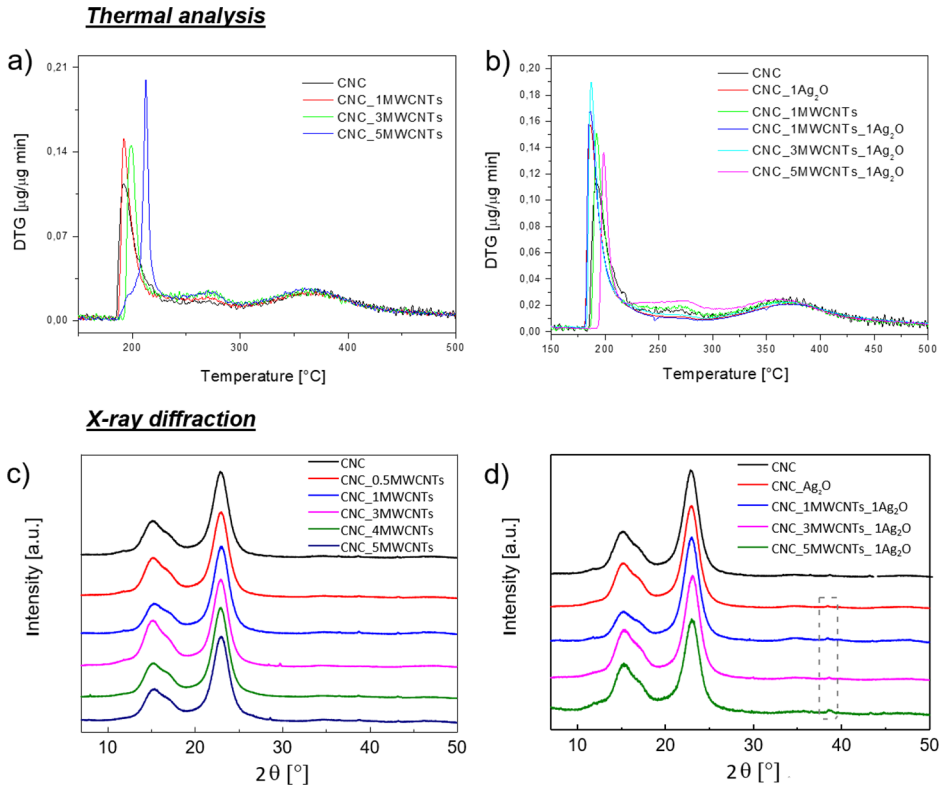

Figure 2. DTG of binary (a) and ternary (b) nanocomposite films in a nitrogen atmosphere. XRD patterns of prepared films: effect of MWCNT concentration (c) and effect of Ag_2O addition (d).

simulation in isothermal−isobaric (NPT) ensemble at 1 atm and 25 °C. All these steps have been repeated for all eight models; finally, the analysis of the MD trajectories has been performed by means of VMD,[37] CHIMERA software,[38] and using tools included in the Gromacs package.

3. RESULTS AND DISCUSSION

3.1. Microstructural Analysis. When dealing with polymer nanocomposites containing MWCNTs, their dispersion within the polymer matrix plays a key role on the resulting physicomechanical performance.[39−42] This is even more relevant in the case of electrical properties, where the percolation threshold (p_c) depends strongly on nanoparticle distribution, i.e., well dispersed nanofillers may yield to an electrically conducting percolated network at lower concentrations.[43,44] Accordingly, MWCNTs distribution over the CNC matrix in both binary CNC/MWCNTs and ternary CNC/MWCNTs/Ag_2O composite films has been investigated through field-emission scanning electron microscopy (FE-SEM). Figure 1A depicts the fracture cross-section of CNC/MWCNTs composite films with a varying concentration up to 5 wt %. When dispersed in water, CNCs isolated upon acid hydrolysis of native cellulose are able to form a nematic liquid crystal phase above a critical concentration.[45,46] This organization shown by CNCs bearing negatively charged functional groups can be captured in solid films after a controlled evaporation-induced self-assembly (EISA). During this process, the aqueous solvent continuously evaporates to yield materials composed by stacked CNC layers, as observed in Figure 1 for the neat CNC film. At the same time, the FE-

https://doi.org/10.1021/acs.jpcc.3c04767
J. Phys. Chem. C XXXX, XXX, XXX−XXX

SEM images of composite films show a similar dense structure of CNCs (with no pores) after MWCNT incorporation, suggesting that the presence of carbon nanotubes in aqueous CNC suspensions does not disrupt the self-assembly process of neat CNC dispersions after water evaporation.

This observation is confirmed by the higher-magnification micrograph of the CNC/MWCNT 5 wt % film in Figure S1a, where nanotubes (highlighted by an arrow) remain well-dispersed within the cellulosic matrix. It can be thus expected that this homogeneous distribution may result in the formation of a physical continuous pathway of interconnected electrically conducting MWCNTs within the cellulosic matrix at relatively low filler concentrations.[47]

Similarly, Figure 1B shows the morphology of the fracture surface of ternary CNC/MWCNTs/Ag_2O composite films. Again, all of the films present a dense structure, with no apparent aggregates of MWCNTs or Ag_2O. Such homogeneous nanoparticle distribution is ascribed to the occurring electrostatic forces when dispersed in water. In particular, when in aqueous solution, the electrostatic forces between adjacent CNC (originating from the negatively charged sulfate half-ester group onto CNC surfaces) are able to keep the composite constituents well-dispersed.[48] Upon drying and subsequent EISA, this well-dispersed structure is "frozen" in the solid state, yielding films with homogeneously distributed nanotubes and silver nanoparticles at the molecular level as occurring with other CNC-based systems.[49,50] Altogether, these observations with also higher-magnification micrograph of the ternary nanohybrid system reported in Figure S1, b, confirm that homogeneously distributed composites have been obtained.

Figure 2a,b shows derivative thermogravimetric (DTG) curves of CNC/MWCNTs (a) and CNC/MWCNTs/Ag_2O (b) nanohybrid films during heating in nitrogen atmosphere as a function of carbon nanotubes content. As already observed in the case of CNC/SWCNTs,[9] thermal degradation of binary nanohybrids was delayed upon the addition of the carbon nanotubes, with an increase in DTG_{max} values (from 0.15 to 0.20%min^{-1}) and a shift of the main degradation event of CNC (measured at 192 °C) to 199 and 213 °C for CNC_3MWCNTs and CNC_5MWCNTs, respectively. This phenomenon results from the typical retardant effect of MWCNTs on the cleavage of the glycosidic linkages of cellulose. The residual weight at 900 °C of CNC (23.4 wt %) exceeds those of all CNC/MWCNTs hybrids (measured as 22.6, 20.8, and 19.3 wt % for CNC_1MWCNTs, CNC_5MWCNTs, and CNC_5MWCNTs, respectively), (Figure S2) which can be ascribed to a large number of free end chains during the acid-hydrolysis process, which have been proven to decompose at a lower temperature, leading to an increase in the char yield of CNC.[51]

In the presence of both MWCNTs and Ag_2O, the nanohybrids demonstrated a reduced thermal stability, which is reflected in a residual weight of 14.8% and a T_{peak} measured at 199 °C for CNC_5MWCNTs_1Ag_2O, with values lower than the ones registered for the same system in the absence of the silver oxide nanoparticles (residual weight of 20.8% and T_{peak} measured at 213 °C for CNC_5MWCNTs). Less evident in the case of the lower amount of MWCNTs (CNC_3MWCNTs and CNC_3MWCNTs_1Ag_2O) registered, residual weights had values of 19.3 and 19.9 wt % and T_{peak} shifted from 199 to 192 °C; however, the decrease was also observed in the binary system CNC_1Ag_2O, with a reduction of the main peak temperature from 192 to 186 °C and a decrease of residual weight from 23.4 to 6.8 wt %, when compared to CNC film. This behavior can be related to the catalytic role of the metallic oxide Ag_2O in the degradation process of both cellulose and carbon based materials.[52,53]

3.2. Physicochemical Properties and Semicrystalline Structure. In order to investigate the effect of MWCNTs and Ag_2O introduction and evaluate synergic interaction between selected nanofillers having different properties, in terms of aspect ratio and chemistry, the interactions between hybrid partners were investigated by infrared spectroscopy. Figure S3 compares the CNC neat film with CNC/MWCNTs and CNC/MWCNTs/Ag_2O, in the 1800−700 cm^{-1} frequency range. The analyzed region shows a large absorption between 1180 and 930 cm^{-1}, due to the contribution of the stretching vibration of (C−C), (C−O), and (C−O−C) functional groups.

All samples show the same peaks at 1034, 1057, and 1259 cm^{-1}.[54,55] Meanwhile, the band near 1320−1210 cm^{-1} associated with the bond stretching of the C−O group shows some difference, mainly in the nanocomposite with silver nanoparticles, even if no new IR absorption peaks were observed, probably due to the low Ag_2O content, under the FT-IR detection limit. However, some changes were observed in the peak located in the 1200−1300 cm^{-1} region, in the FT-IR spectra of the CNC-based nanocomposites, which can be due to the interaction of the Ag_2O nanoparticles and MWCNTs with the cellulose nanocrystals.[56]

The crystalline structure of the composite films was investigated by powder X-ray diffraction (XRD). Figure 2c,d presents the XRD patterns of binary CNC/MWCNTs (Figure 2c) and ternary CNC/MWCNTs/Ag_2O (Figure 2d) composites. All the films display broad diffraction peaks corresponding to the $(\bar{1}10)$, (101), and (200) planes of cellulose I located at 2θ = 14.9, 16.5, and 22.7°, respectively (an additional weak peak arising from the (004) plane is seen at 2θ = 34.4°).[57,58] The well-known characteristic diffraction peaks of MWCNTs at 2θ = 26 and 43° originating from the (002) and (100) planes of the hexagonal graphite, respectively,[59,60] are not observed due to their low concentration within the composite film. Conversely, a low intensity reflection at 2θ = 38.2° arising from the (200) plane of the face-center cubic Ag_2O could be seen (whose intensity increases with Ag_2O concentration, highlighted in gray), indicating the presence of such nanoparticles within the composite films.[61] Overall, composite films do not change the diffraction pattern of CNC for the different processing conditions and compositions, implying that the original semicrystalline character or CNC is preserved during processing.

3.3. Electrical and Dielectrical Properties of Hybrid Nanocomposites. To investigate the electric properties of the hybrid binary and ternary CNC-based films, results for voltage-dependent electric current in the thickness direction of the films fabricated with different MWCNT content and under different humidity conditions were obtained. In the current−voltage (I−V) curves (data not shown), no electric current change is detected for the neat CNC film. On the other hand, for all the hybrid cellulose films, the electric current increases linearly with the applied voltage. It is worth noting that nanocellulose itself is not a conductor; thus, neat nanocellulose films exhibit low conductivity.[9] The dispersion of MWCNTs improves the conductivity, even at low MWCNT contents as the nanofillers are individually dispersed; hence, a conductive

https://doi.org/10.1021/acs.jpcc.3c04767
J. Phys. Chem. C XXXX, XXX, XXX−XXX

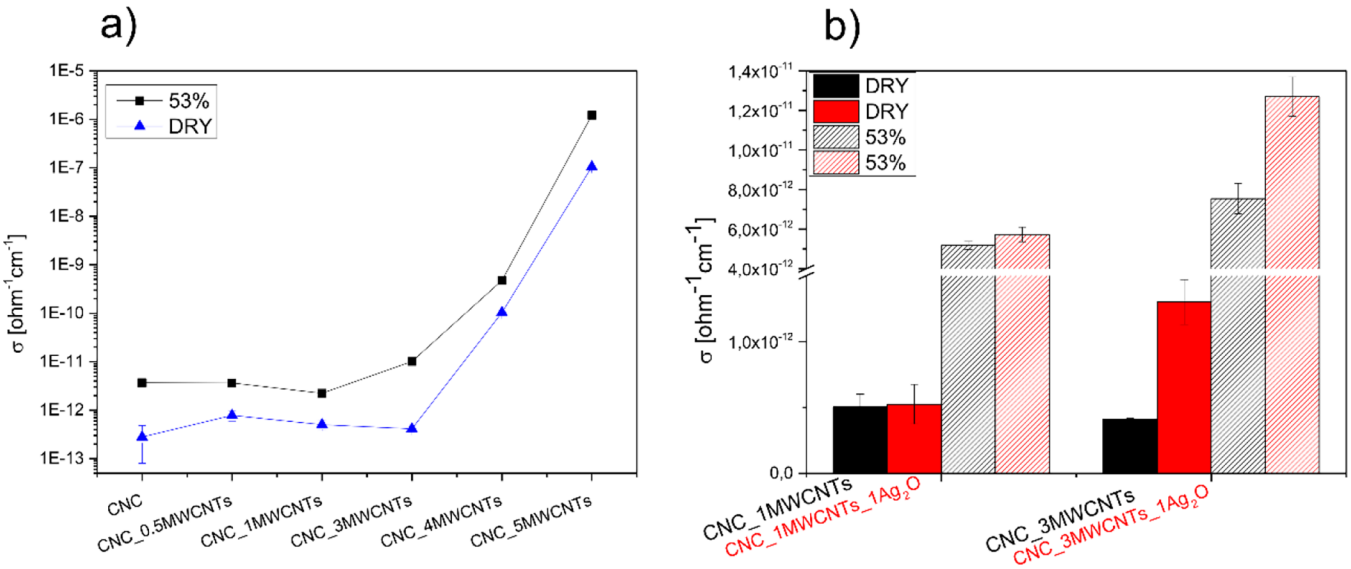

Figure 3. DC electrical conductivity of CNC and CNC/MWCNTs films (a); CNC/MWCNTs and CNC/MWCNTs/Ag_2O films (b) at different weight contents measured in the dry state and in wet environment conditions (RH = 53%).

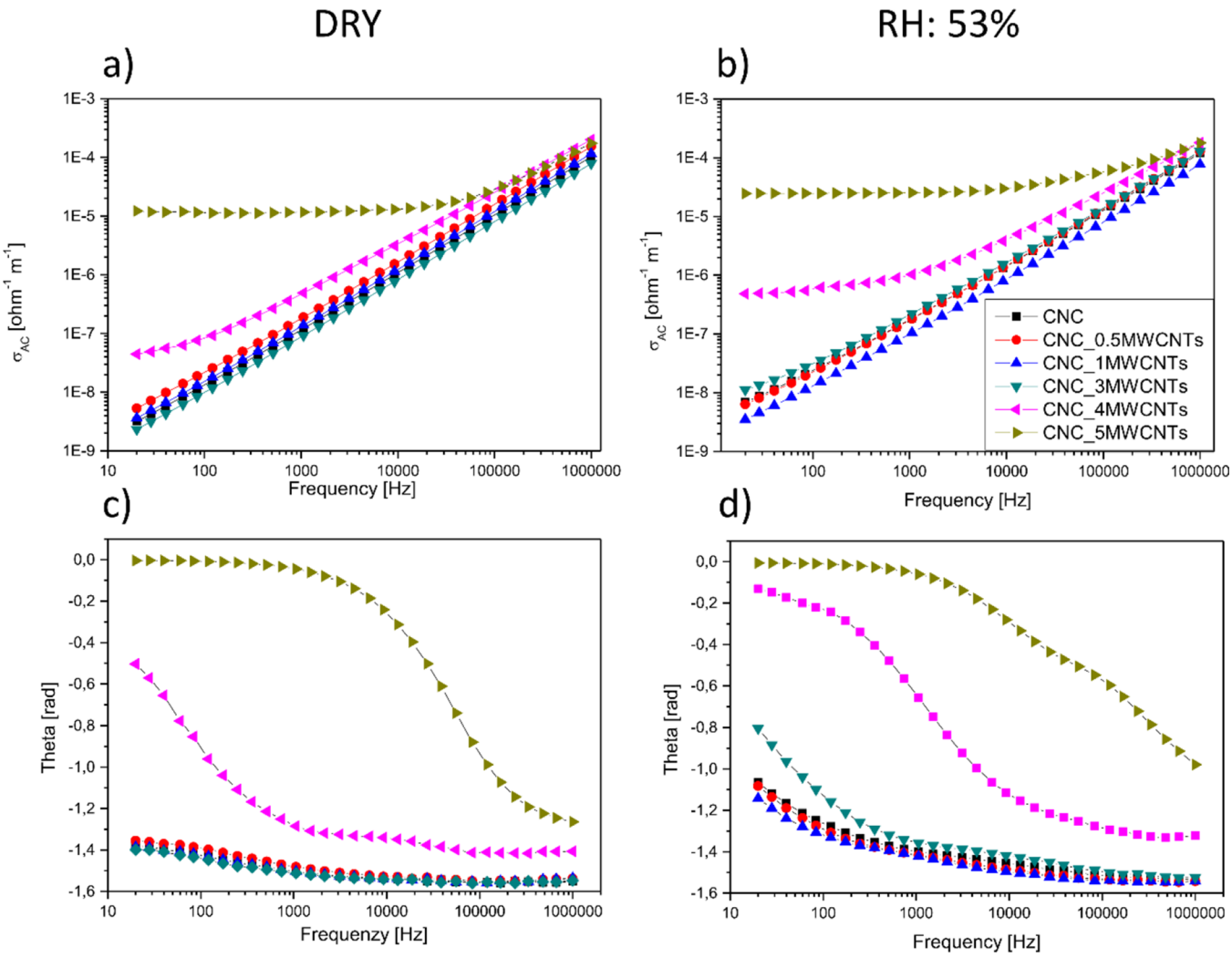

Figure 4. Frequency dependence of the AC conductivity (a, b) and phase angle (c, d) for different CNC films at varying MWCNT content, in the 20 Hz−1 MHz frequency range, measured in dry conditions (a, c) and humidity fixed at 53% (b, d).

https://doi.org/10.1021/acs.jpcc.3c04767
J. Phys. Chem. C XXXX, XXX, XXX−XXX

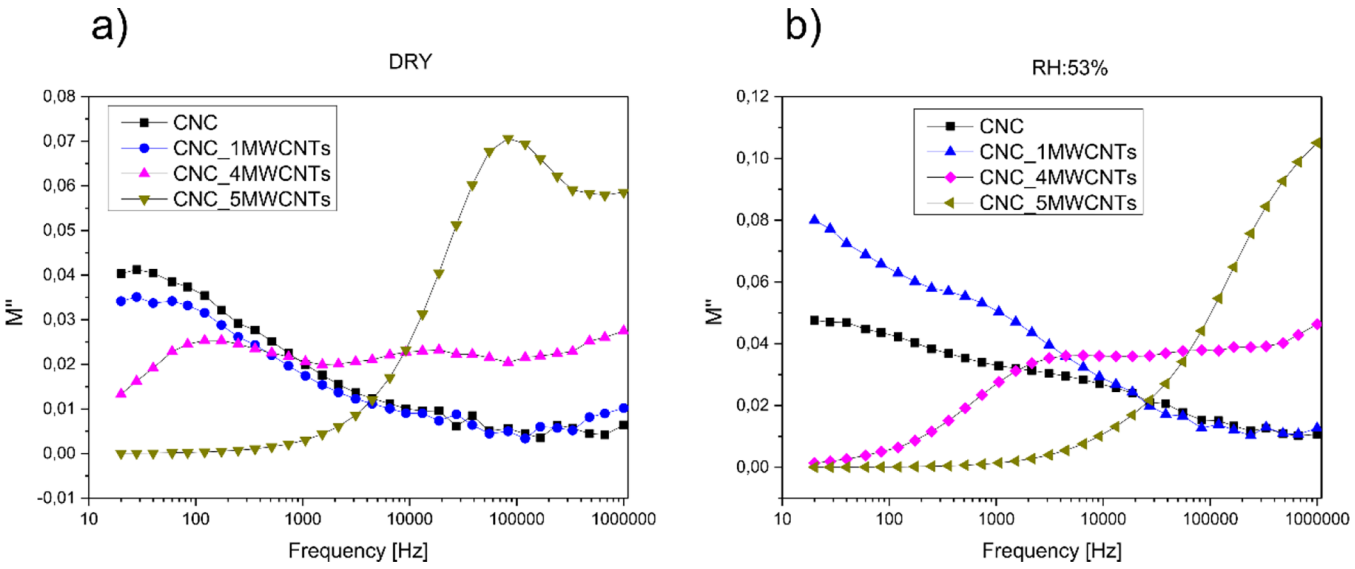

Figure 5. Frequency dependence of the imaginary part of modulus (M'') in the 20 Hz−1 MHz frequency range, measured in dry (a) and wet environments (RH:53%) (b).

network has not been formed and the electric charge cannot effectively flow. By increasing the MWCNT content (up to 3 wt %), the conductivity improves significantly, as reflected in Figure 3a. The same behavior was observed in the case of binary films based on CNC and SWCNTs, even if in this case, the percolation threshold was obtained for lower SWCNT content.[9] Figure 3a shows a comparison of the conductivity with the same MWCNT content at different humidity conditions. The properties of cellulose-based materials are strongly related to their water content. Therefore, the effect of the water content cannot be ignored in the study. As shown in Figure 3b, the DC conductivity of the film enhances with the increase of relative humidity. Adsorbed water may act in the binary films as a plasticizer, inducing the formation of a better organized and denser network.[9] The presence of silver oxide nanoparticles (Figure 3b) slightly improves the DC conductivity in the dry state and in the 53% RH condition. This effect is more pronounced in the case of larger content of MWCNTs. Silver oxide nanoparticles can act as conductive bridges among MWCNT bundles and facilitate the formation of conductive pathways and the electron transfer in the multifunctional films, as previously demonstrated in the case of a thermoplastic polymer.[62]

Impedance spectroscopy measurements were also performed on binary and ternary films in the thickness direction in the dry state and at 53% of relative humidity. Figure 4 reports the AC conductivity and phase angle of binary samples realized with an increased content of MWCNTs. Figure 4a,b reports the evolution of the AC electrical conductivity in the frequency range (20 Hz to 1 MHz) for the binary films at the different MWCNT weight contents, from 0.5 to 5 wt %, and for the neat CNC for comparison. In the analyzed frequency range, when the MWCNT content is below the percolation threshold (i.e., 3 wt %), an evident frequency-dependent behavior similar to that observed for the neat CNC film is detected. Increasing the MWCNT content at 4 wt %, a different trend was observed, with a progressive increase of the AC conductivity at low frequency, with a frequency-independent behavior that is typical of disordered insulator−conductor mixtures. An evident transition from a frequency independent conductivity, close to that in direct current, to a frequency-dependent behavior starting from a critical frequency f_c, as observed for the electrical impedance, was detected. After this frequency, the AC conductivity ($\sigma(\omega)$) increases with a behavior that, in the whole frequency range, can be described by the power law.[25]

At low frequencies, the frequency-independent conductivity is DC conductivity, while at high frequencies, the AC conductivity is enhanced due to the excess of generated charge carriers. Figure 4c,d reports the phase angle behavior; coherently with our previous works[25,9] and, as expected for an insulating material that acts as a capacitor, for neat CNC and for film whose MWCNTs loadings is below the percolation threshold, the phase angle $\cong -1$ rad, with a frequency-independent behavior. Increasing the MWCNT content, the phase evolves from zero. From an electric point of view, this means that at low frequency, the overall impedance of percolated material is mainly due to the resistive term, whereas at higher frequencies, it is mainly determined by the capacitive effects of materials: the reactance associated with the capacitor decreases, reaching values lower than the resistance exhibited by the nanohybrid.

3.4. Modulus Formalism. The conductivity of the CNC-based film depends on the concentration and mobility of the conductive species and interface properties. In nanohybrid systems, interfacial polarization is almost always present due to additives, fillers, or even impurities that make these systems heterogeneous. Usually, in systems with a conductive component, interfacial polarization is obscured by the conductivity, and the dielectric permittivity can be very high at low frequencies. To overcome this difficulty, the modulus formalism has been widely used to analyze the electrical conductivity data in ionic conductors and polymers despite an ongoing controversy on its applicability.[63] The experimental dielectric spectroscopy measurements and the transport electrical measurements have been analyzed also by using the electric modulus formalism,[63,64] in order to better explain the interphase properties of the binary and ternary CNC-based materials and well understand the water interaction. The complex dielectric modulus (M^*) is defined as

https://doi.org/10.1021/acs.jpcc.3c04767
J. Phys. Chem. C XXXX, XXX, XXX−XXX

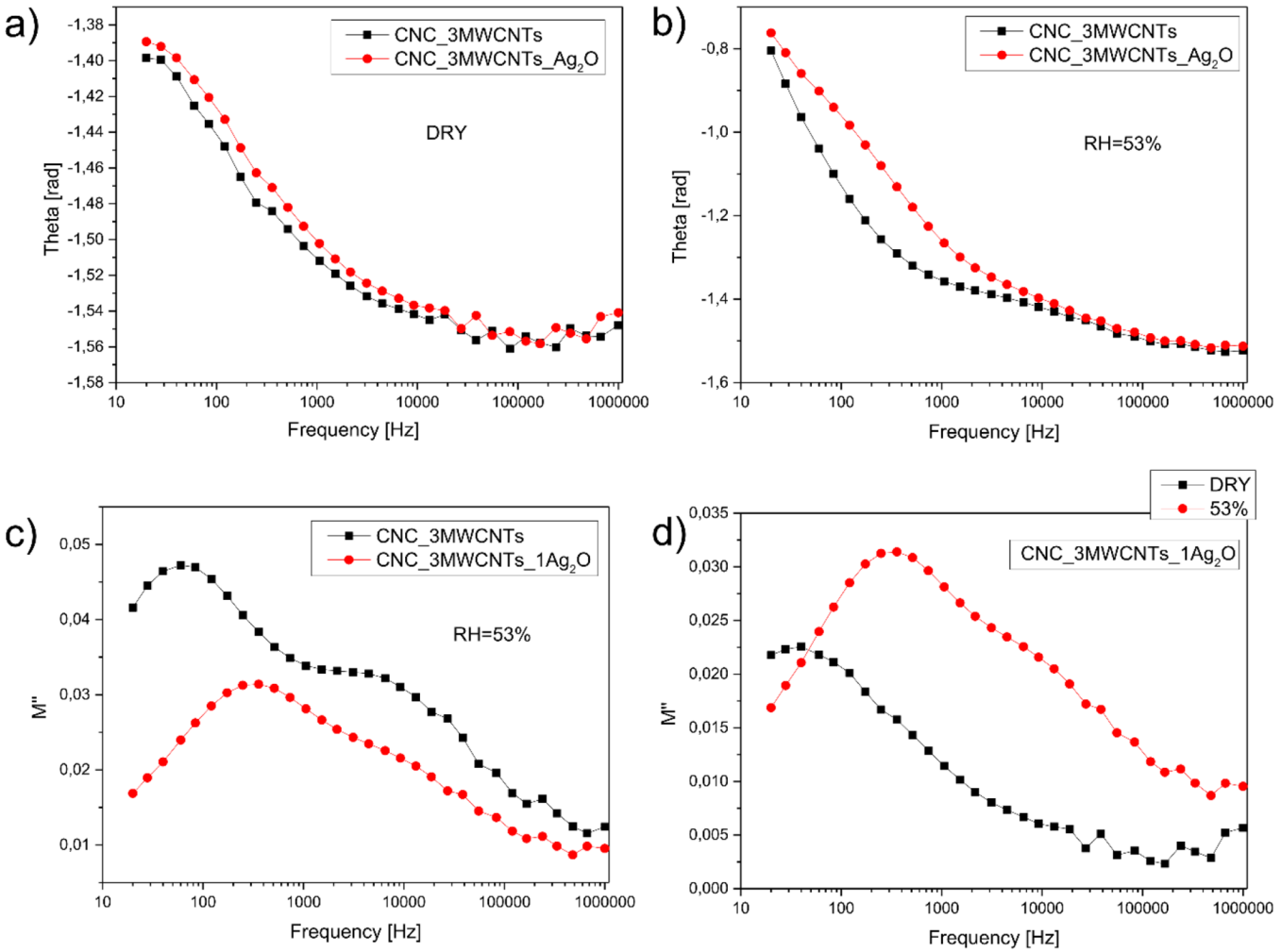

Figure 6. Role of the silver oxide nanoparticles of phase angle (a, b) and frequency dependence of the imaginary part of modulus (M'') (c, d) in the 20 Hz−1 MHz frequency range, measured dry (a) and in humidity fixed at 53% (b, c). Effect of humidity conditions in ternary composites (d).

$$M^* = \frac{1}{\epsilon^*} = \frac{\epsilon'}{\epsilon'^2 + \epsilon''^2} + i\frac{\epsilon''}{\epsilon'^2 + \epsilon''^2} \quad (2)$$

$$M^* = M' + iM'' \quad (3)$$

where M' and M'' are the real and imaginary parts of the electric modulus, respectively. The complex modulus permits one to study the interfacial polarization and emphasize small features at small frequencies, almost always present in heterogeneous systems as CNC-based nanohybrids. In particular, in systems with conductive nanofillers as MWCNTs, interfacial polarization cannot well be visible for the high conductivity; hence, the dielectric permittivity at low frequencies and electric modulus permit to overcome this problem.

Figure 5 shows the frequency dependence of the imaginary part of the dielectric modulus (M'') of the binary CNC/MWCNTs films for selected weight content, in the dry state (a) and at 53% relative humidity (b). In Figure 5a, a characteristic peak related to the transition region (from DC to AC conductivity) could be recognized for the sample with high MWCNT loading. For the nanocomposite with 1 wt %, it is located a bit lower the experimental frequency window, whereas for the neat CNC, it is out of the frequency window. At 53% of relative humidity, a shift of the peak at higher frequency can be observed (Figure 5b and Figure S4a−c).

The electric modulus representation shows well-defined relaxation peaks. In the M'' plot, the peaks are asymmetric on both sides of the maxima and broader than predicted by the ideal Debye behavior. The frequency range where the peak occurs is the indication of a transition from long-range to short-range mobility. The frequency at which the maximum of M'' (M''_{max}) occurs defines the relaxation time τ_c by the relation $\tau_c\omega_c = 1$. The peak in the M'' plot shifts toward higher frequencies with increasing weight content of conductive nanofillers. The asymmetric M'' plot is suggestive of the stretched exponential character of relaxation times of the material. The stretched exponential function is defined by the empirical Kohlrausch−Williams−Watts (KWW) function.

The silver oxide nanoparticle introduction at 1 wt % does not affect the AC conductivity behavior at the selected MWCNT content (3 wt %), while the phase angle curves are slightly changed (Figure S5a,b). In dry state (Figure 6a), the curves show the same behavior, while at 53% of humidity, the silver oxide nanoparticle addition improves the band at lower frequency, indicating a different water interaction mechanism with the ternary nanohybrid film (Figure 6b). Silver oxide nanoparticle introduction was also analyzed by the modulus formalism (Figure 6c,d). The electric modulus representation shows well-defined broad peaks; the asymmetric nature of the curve and the broad M'' peaks can be explained as being the

https://doi.org/10.1021/acs.jpcc.3c04767
J. Phys. Chem. C XXXX, XXX, XXX−XXX

result of the distribution of relaxation time and deviation from the ideal Debye type. Furthermore, a shift of the peak at higher frequency was observed with silver oxide nanoparticle introduction and this effect was improved at 53% of humidity. This shift implies that as water molecules interact with the nanohybrid systems the relaxation time decreases.

3.5. MD Simulations of Cellulose Nanocrystal Ternary Films Based on MWCNTs and Silver Oxide Nanoparticles. With the aim to describe in detail the interactions on the interfaces between different components, MD simulations have been carried out, and the models without water have been first discussed. The molecular modeling at the atomic level and the dynamical description with computational methods are helpful to provide a more complete view about the characteristics of the cellulose nanocrystals, which are known to be correlated to the reactivity of the carboxyl and hydroxyl groups of the biopolymers' chains.[65]

CNC showed high stability along the MD simulation, suggesting that the modeled nanocrystal (Figure 7a) was stable

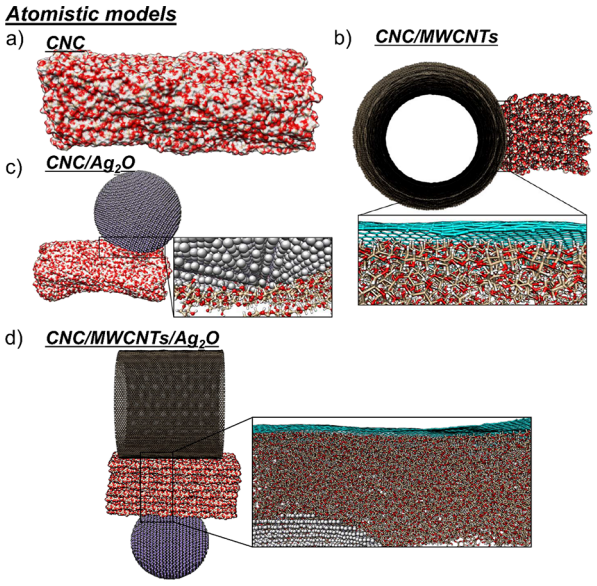

Figure 7. Surface model of CNC obtained after 100 MD simulations (a). Atomistic model of: CNC/MWCNT (b), CNC/Ag_2O NP (c) and CNC/MWCNTs/Ag_2O (d). O, C, and H atoms of CNC are highlighted in red, brown, and white colors, respectively, The C atoms of MWCNT in the focus are reported in cyan, and the atoms of Ag_2O are reported in gray.

and suitable for the comparisons with the experimental evidence. Analyzing the CNC/MWCNTs, stable interactions between the cellulose and the nanotube have been detected along the whole simulation time. In detail, a very stable complex has been found, with many interactions on the surfaces of different materials (Figure 7b). Analyzing the trajectories, the CNC oriented its surface to promote interactions between its apolar groups and the electron cloud of the MWCNTs. The capabilities of cellulose nanocrystals to adhere on graphene surface via apolar interactions has been already observed.[66,67]

In the CNC/Ag_2O system, stabilizing interactions have been observed between the nanocrystal and the Ag_2O NPs, but in this case, the type of interaction was different with respect to those previously described. The high amount of Ag^+ ions in the system led to strong interactions with the polar groups of CNC. Along MD simulation, $^-$OH groups of nanocrystals oriented themselves to favor ion−dipole interactions with Ag^+ ions and on the same time generating hydrogen bonds with the O atoms present in the Ag_2O NP (Figure 7c).

Focusing on the CNC/MWCNTs/Ag_2O system, a stable complex has been observed again. The previously described interactions, which involve the CNC apolar groups with MWCNTs and the CNC polar groups with the Ag_2O system, coexist in this model. In fact, along MD simulations, the nanotube and the Ag_2O based particle disposed themselves in the two opposite sides of the simulation box, generating a sort of bridge in which CNC interacts with both systems by using two opposite surfaces (Figure 7d). The effect of the water in the interactions has also been investigated. As previously reported, the amount of the water molecule to add for reaching an RH of 50% is related to the dimension of the simulation box, and then, a different amount of water molecule has been included. The number of the water molecules on the surface has been calculated for each system during the 100 ns of MD simulations, allowing to quantify the adsorption of the water in different systems and to clarify the role of different components on this phenomenon. Starting from the behavior of the only CNC, this system resulted able to adsorb a small amount of water molecules as already reported in the literature.[68] Estimating the number of molecules directly interacting with the interface of CNC through H bonds, a total of 1360 molecules have been adsorbed by cellulose (Figure 8a), which correspond to an adsorption of 2.26%.

Even if MWCNTs and Ag_2O NPs do not adsorb water, the presence of H_2O at the CNC interface should reflect different interactions when these systems are present. For these reasons, all these systems have been investigated. MD inspections showed that in the CNC/MWCNTs system, water molecules oriented themselves on the interface between the two components (Figure 8b); however, opposite effects have been observed. From one side, cellulose interacts with water through hydrogen bonding, as previously reported in line with the literature.[65] On the other hand, the interaction between CNC and MWCNT has a hydrophobic nature, and for this reason, water molecules have been displaced between CNC/MWCNT surfaces. These counteracting effects led to a disordered fluctuations of water molecules between these two systems, meaning that the hydrogen bonding between CNC and water together with the hydrophobic effects between CNC and MWCNT played a crucial role in the balance of entropic and enthalpic effects along MD simulations.[67]

A crucial role of the water has been also identified in the presence of Ag_2O NP. In this case, since stabilizing ion−dipole interactions have been observed between CNC and Ag_2O NP, the H_2O molecules adsorbed from CNC disposed themselves between the two components in a more ordered way with respect to the CNC/MWCNT system. In fact, no counteracting effects have been detected in the presence of Ag_2O, and water molecules promoted a bridge between the polar OH groups of the CNC and the polar parts of NPs, composed by Ag^+ and O^{2-} ions (Figure 8c).

Finally, a CNC/MWCNTs/Ag_2O complex has been detected also in the presence of water. This is true since water molecules were uniformly distributed on the CNC surface, and MWCNT and Ag_2O interact with the cellulose using two opposite positions, as previously observed. This aggregate exhibited the same characteristics of the corresponding one without water, in which the cellulose was oriented in

https://doi.org/10.1021/acs.jpcc.3c04767
J. Phys. Chem. C XXXX, XXX, XXX−XXX

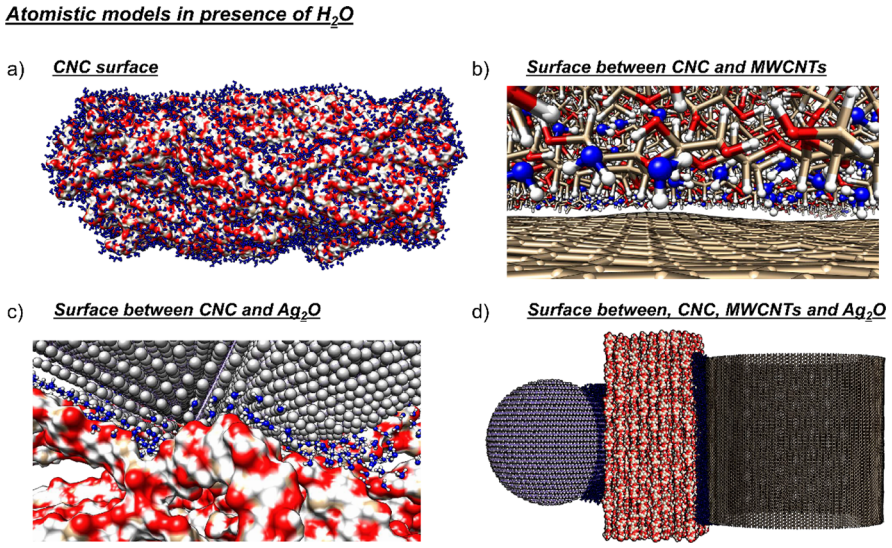

Figure 8. CNC surface and the adsorbed water molecules (a). Interface between: CNC and MWCNTs (b), CNC and Ag_2O NP (c), CNC with Ag_2O NP, and MWCNT Ag_2O NP (d) in the presence of water molecules. O, C, and H atoms of CNC are highlighted in red, brown, and white colors, respectively. MWCNTs and Ag_2O components are reported in brown and in gray, and water molecules are evidenced with blue and white.

the middle and the Ag_2O and the MWCNT were in two opposite sides between them. The only one difference is associated with the role of the water. In fact, H_2O was disposed on the CNC/Ag_2O interface in an ordered manner, and at the same time, higher water fluctuations have been detected on CNC/MWCNT surface. All of the previously described interactions between the different materials have been observed, following the previously described behaviors (Figure 8d) and leading to the formation of a more organized net. The orientation in an ordered manner of water molecules in the presence of silver oxide nanoparticles well explain the improvement of electrical properties with increasing in electrical conductivities and the shift at higher frequencies of electrical modulus, due to the faster molecule movements leading to the decrease in the relaxation times.

4. CONCLUSIONS

This work investigated the influence of the MWCNT dispersion in CNC polymer films and the combined effect of silver oxide nanoparticles on the electrical and dielectrical properties of the CNC-based films. Electron microscopy observations show a homogeneously distributed MWCNT and Ag_2O NPs within the nanocellulosic host. The added nanoparticles have opposite effects in terms of thermal stability, while the carbon nanotubes act as physical barriers to prevent permeation of degradation products through the material and outward (manifested in a 21 °C sight of the main thermodegradation event), the Ag_2O nanoparticles act as a catalyst to accelerate the cleavage of glycosidic linkages of cellulose, lowering the main thermodegradation temperature by 6 °C. As expected, 5 wt % MWCNTs increase the DC electrical conductivity of neat CNC films by 7 orders of magnitude. In addition, silver oxide nanoparticles also enhance the DC conductivity, both in the dry state and in the 53% RH condition, providing the occurrence of synergetic events. The AC conductivity and dielectric behavior of binary and ternary CNC-based conductive films have been studied as a function of frequency, and the charge transport properties have been investigated as a function of humidity conditions. MD simulations revealed different interactions of MWCNTs and Ag_2O NPs with CNC, and moreover, these interactions never competed between them, confirming the uniform dispersion of these materials in CNC films. Additionally, the amount of water adsorption on CNC surface has been estimated, leading to an adsorption of 2.26%. Finally, few water molecules have been found between the interfaces, remarking the crucial role of the solvent in the determination of a more organized net with oriented molecules between CNC/Ag_2O interface, while a more entropic factor associated with the solvent has been detected on CNC/MWCNT. The simulation results here reported could help to explain the increase in the electrical conductivity of cellulosic-materials measured experimentally, not only in the presence of inorganic nanoparticles such as carbon nanotubes and silver oxide but also in the presence of water molecules.

■ ASSOCIATED CONTENT

Data Availability Statement

All the data used to support the findings of this study are included within the article.

Supporting Information

The Supporting Information is available free of charge at https://pubs.acs.org/doi/10.1021/acs.jpcc.3c04767.

High magnification FE-SEM images, TGA traces, FTIR spectroscopy, and modulus formalism on the effect of humidity on electrical properties (PDF)

■ AUTHOR INFORMATION

Corresponding Author

Ilaria Armentano − *Department of Economics, Engineering, Society and Business Organization (DEIM), University of Tuscia, Largo dell'Università snc, Viterbo 01100, Italy;* orcid.org/0000-0002-8266-4366; Email: ilaria.armentano@unitus.it

Authors

Francesca Luzi − *Department of Science and Engineering of Matter, Environment and Urban Planning (SIMAU), Polytechnic University of Marche, Ancona 60131, Italy*

https://doi.org/10.1021/acs.jpcc.3c04767
J. Phys. Chem. C XXXX, XXX, XXX−XXX

Ainhoa Angulo Dehesa − *Department of Graphic Design and Engineering Projects. Faculty of Engineering in Bilbao, University of the Basque Country (UPV/EHU), Bilbao 48013, Spain; Civil and Environmental Engineering Department, UdR INSTM, University of Perugia, Terni 05100, Italy*

Emiliano Laudadio − *Department of Science and Engineering of Matter, Environment and Urban Planning (SIMAU), Polytechnic University of Marche, Ancona 60131, Italy;* orcid.org/0000-0002-8053-6539

Debora Puglia − *Civil and Environmental Engineering Department, UdR INSTM, University of Perugia, Terni 05100, Italy;* orcid.org/0000-0001-8515-7813

Erlantz Lizundia − *Department of Graphic Design and Engineering Projects. Faculty of Engineering in Bilbao, University of the Basque Country (UPV/EHU), Bilbao 48013, Spain; BCMaterials, Basque Center for Materials, Applications and Nanostructures, UPV/EHU Science Park, Leioa 48940, Spain*

Pierluigi Stipa − *Department of Science and Engineering of Matter, Environment and Urban Planning (SIMAU), Polytechnic University of Marche, Ancona 60131, Italy*

Luigi Torre − *Civil and Environmental Engineering Department, UdR INSTM, University of Perugia, Terni 05100, Italy*

Complete contact information is available at: https://pubs.acs.org/10.1021/acs.jpcc.3c04767

Author Contributions

#A.A.D. and F.L. did equal contribution to this work

Author Contributions

F.L. and A.A.D. did the investigation and methodology; E.La. performed the validation and methodology; D.P. did the formal analysis and writing—original draft; E.Li. did the conceptualization, writing, and funding acquisition; P.S. and L.T. acquired funding; and I.A. did the conceptualization, supervision, and writing—original draft, review, and editing.

Notes

The authors declare no competing financial interest.

■ ACKNOWLEDGMENTS

A.A.D. thanks GARAPEN (Basque Association of Development Agencies) for the Global Training grant. Technical and human support provided by SGIker (UPV/EHU, MICINN, GV/EJ, EGEF, and ESF) is gratefully acknowledged. The authors also acknowledge the funds from the University of the Basque Country (Convocatoria de ayudas a grupos de investigacion GIU21/010).

■ REFERENCES

(1) Calle-Gil, R.; Castillo-Martínez, E.; Carretero-González, J. Cellulose Nanocrystals in Sustainable Energy Systems. *Adv. Sustainable Syst.* **2022**, *6* (4), 2100395.

(2) Scaffaro, R.; Maio, A.; Gammino, M. Hybrid biocomposites based on polylactic acid and natural fillers from *Chamaerops humilis* dwarf palm and *Posidonia oceanic* leaves. *Adv. Compos Hybrid Mater.* **2022**, *5*, 1988−2001.

(3) More, A. P. Flax fiber−based polymer composites: a review. *Adv. Compos Hybrid Mater.* **2022**, *5*, 1−20.

(4) Lian, M.; Huang, Y.; Liu, Y.; Jiang, D.; Wu, Z.; Li, B.; Xu, Q.; Murugadoss, V.; Jiang, Q.; Huang, M. An overview of regenerable wood-based composites: preparation and applications for flame retardancy, enhanced mechanical properties, biomimicry, and transparency energy saving. *Adv. Compos Hybrid Mater.* **2022**, *5*, 1612−1657.

(5) Lizundia, E.; Puglia, D.; Nguyen, T.-D.; Armentano, I. Cellulose Nanocrystal Based Multifunctional Nanohybrids. *Prog. Mater. Sci.* **2020**, *112*, 100668.

(6) Vincent, S.; Kandasubramanian, B. Cellulose Nanocrystals from Agricultural Resources: Extraction and Functionalisation. *Eur. Polym. J.* **2021**, *160*, 110789.

(7) Trache, D.; Hussin, M. H.; Haafiz, M. K. M.; Thakur, V. K. Recent Progress in Cellulose Nanocrystals: Sources and Production. *Nanoscale* **2017**, *9* (5), 1763−1786.

(8) Lizundia, E.; Goikuria, U.; Vilas, J. L.; Cristofaro, F.; Bruni, G.; Fortunati, E.; Armentano, I.; Visai, L.; Torre, L. Metal Nanoparticles Embedded in Cellulose Nanocrystal Based Films: Material Properties and Post-Use Analysis. *Biomacromolecules* **2018**, *19* (7), 2618−2628.

(9) Dehesa, A. A.; Luzi, F.; Puglia, D.; Lizundia, E.; Armentano, I.; Torre, L. Effect of SWCNT Content and Water Vapor Adsorption on the Electrical Properties of Cellulose Nanocrystal-Based Nanohybrids. *J. Phys. Chem. C* **2020**, *124* (27), 14901−14910.

(10) Zhang, H. C.; Yu, C. N.; Li, X. Z.; Wang, L. F.; Huang, J.; Tong, J.; Lin, Y.; Min, Y.; Liang, Y. Recent Developments of Nanocellulose and its Applications in Polymeric Composites. *ES Food Agrofor.* **2022**, *9*, 1−14.

(11) Gu, H.; Huo, X.; Chen, J.; M. El-Bahy, S.; M. El-Bahy, Z. An Overview of Cellulose Aerogel: Classification and Applications. *ES Food Agrofor.* **2022**, *10*, 1−9.

(12) Lee, Y.; Zhang, H.; Yu, H. Y.; Tam, K. C. Electroconductive cellulose nanocrystals — Synthesis, properties and applications: A review. *Carb Polym.* **2022**, *289*, 119419.

(13) Qu, K.; Sun, Z.; Shi, C.; Wang, W.; Xiao, L.; Tian, J.; Huang, Z.; Guo, Z. Dual-acting cellulose nanocomposites filled with carbon nanotubes and zeolitic imidazolate framework-67 (ZIF-67)−derived polyhedral porous Co_3O_4 for symmetric supercapacitors. *Adv. Compos. Hybrid Mater.* **2021**, *4*, 670−683.

(14) Li, Y.; Guo, J.; Li, M.; Tang, Y.; Murugadoss, V.; Seok, I.; Yu, J.; Sun, L.; Sun, C.; Luo, Y. Recent Application of Cellulose Gel in Flexible Sensing-A Review. *ES. Food Agrofor.* **2021**, *4*, 9−27.

(15) Durairaj, A.; Maruthapandi, M.; Saravanan, A.; Luong, J. H. T.; Gedanken, A. Cellulose Nanocrystals (CNC)-Based Functional Materials for Supercapacitor Applications. *Nanomaterials* **2022**, *12* (11), 1828.

(16) Zhu, L.; Zhou, X.; Liu, Y.; Fu, Q. Highly Sensitive, Ultrastretchable Strain Sensors Prepared by Pumping Hybrid Fillers of Carbon Nanotubes/Cellulose Nanocrystal into Electrospun Polyurethane Membranes. *ACS Appl. Mater. Interfaces* **2019**, *11* (13), 12968−12977.

(17) Cao, Y.; Zeng, Z.; Huang, D.; Chen, Y.; Zhang, L.; Sheng, X. Multifunctional Phase Change Composites Based on Biomass/MXene-Derived Hybrid Scaffolds for Excellent Electromagnetic Interference Shielding and Superior Solar/Electro-Thermal Energy Storage. *Nano Res.* **2022**, *15* (9), 8524−8535.

(18) Xie, P.; Shi, Z.; Feng, M.; Kai, S.; Yao, L.; Kelan, Y.; Chunzhao, L.; Tarek, M. A. A.; Meina, H.; Shuwei, M. Recent advances in radio-frequency negative dielectric metamaterials by designing heterogeneous composites. *Adv. Compos Hybrid Mater.* **2022**, *5*, 679−695.

(19) Liu, M.; Wu, H.; Wu, Y.; Xie, P.; Adel Pashameah, R.; Abo-Dief, H. M.; El-Bahy, S. M.; Wei, Y.; Li, G.; Li, W. The weakly negative permittivity with low-frequency-dispersion behavior in percolative carbon nanotubes/epoxy nanocomposites at radio-frequency range. *Adv. Compos Hybrid Mater.* **2022**, *5*, 2021−2030.

(20) Lu, Y.; Liu, H.; Gao, R.; Xiao, S.; Zhang, M.; Yin, Y.; Wang, S.; Li, J.; Yang, D. Coherent-Interface-Assembled Ag_2O-Anchored Nanofibrillated Cellulose Porous Aerogels for Radioactive Iodine Capture. *ACS Appl. Mater. Interfaces* **2016**, *8* (42), 29179−29185.

(21) Kwon, S.; Lee, W.; Choi, J. W.; Bumbudsanpharoke, N.; Ko, S. A Facile Green Fabrication and Characterization of Cellulose-Silver Nanoparticle Composite Sheets for an Antimicrobial Food Packaging. *Front Nutr* **2021**, *8*, 778310.

(22) Deshmukh, A. R.; Dikshit, P. K.; Kim, B. S. Green in Situ Immobilization of Gold and Silver Nanoparticles on Bacterial Nanocellulose Film Using Punica Granatum Peels Extract and Their Application as Reusable Catalysts. *Int. J. Biol. Macromol.* **2022**, *205*, 169−177.
(23) Liu, H.; Du, H.; Zheng, T.; Liu, K.; Ji, X.; Xu, T.; Zhang, X.; Si, C. Cellulose Based Composite Foams and Aerogels for Advanced Energy Storage Devices. *Chem. Eng. J.* **2021**, *426*, 130817.
(24) Iijima, S. Helical Microtubules of Graphitic Carbon. *Nature* **1991**, *354* (6348), 56−58.
(25) Monti, M.; Armentano, I.; Faiella, G.; Antonucci, V.; Kenny, J. M.; Torre, L.; Giordano, M. Toward the Microstructure−Properties Relationship in MWCNT/Epoxy Composites: Percolation Behavior and Dielectric Spectroscopy. *Compos. Sci. Technol.* **2014**, *96*, 38−46.
(26) Li, L.; He, M.; Feng, Y.; Wei, H.; You, X.; Yu, H.; Wang, Q.; Wang, J. X. Adsorption of xanthate from aqueous solution by multilayer graphene oxide: an experimental and molecular dynamics simulation study. *Adv. Compos. Hybrid Mater.* **2021**, *4*, 725−732.
(27) Hu, F.; Wang, L.; Liu, Y.; Hessien, M. M.; El Azab, I. H.; Jing, S.; Elnaggar, A. Y.; El-Bah, S. M.; Huang, M.; Zhang, R. Molecular dynamics simulation and experimental study of 3,5-difluoro-2,4,6-trinitroanisole/2,4,6,8,10,12-hexanitrohexaazaisowurtzitane mixed components. *Adv. Compos. Hybrid Mater.* **2022**, *5*, 1307−1318.
(28) Fortunati, E.; Armentano, I.; Zhou, Q.; Iannoni, A.; Saino, E.; Visai, L.; Berglund, L. A.; Kenny, J. M. Multifunctional Bionanocomposite Films of Poly(Lactic Acid), Cellulose Nanocrystals and Silver Nanoparticles. *Carbohydr. Polym.* **2012**, *87* (2), 1596−1605.
(29) Fortunati, E.; Puglia, D.; Luzi, F.; Santulli, C.; Kenny, J. M.; Torre, L. Binary PVA Bio-Nanocomposites Containing Cellulose Nanocrystals Extracted from Different Natural Sources: Part I. *Carbohydr. Polym.* **2013**, *97* (2), 825−836.
(30) Abraham, M. J.; Murtola, T.; Schulz, R.; Páll, S.; Smith, J. C.; Hess, B.; Lindahl, E. GROMACS: High Performance Molecular Simulations through Multi-Level Parallelism from Laptops to Supercomputers. *SoftwareX* **2015**, *1−2*, 19−25.
(31) Huang, J.; Rauscher, S.; Nawrocki, G.; Ran, T.; Feig, M.; de Groot, B. L.; Grubmüller, H.; MacKerell, A. D. CHARMM36m: An Improved Force Field for Folded and Intrinsically Disordered Proteins. *Nat. Methods* **2017**, *14* (1), 71−73.
(32) Darden, T.; York, D.; Pedersen, L. Particle Mesh Ewald: An N·log(N) Method for Ewald Sums in Large Systems. *J. Chem. Phys.* **1993**, *98* (12), 10089−10092.
(33) Páll, S.; Hess, B. A Flexible Algorithm for Calculating Pair Interactions on SIMD Architectures. *Comput. Phys. Commun.* **2013**, *184* (12), 2641−2650.
(34) Eastwood, J. W.; Hockney, R. W.; Lawrence, D. N. P3M3DP—The Three-Dimensional Periodic Particle-Particle/ Particle-Mesh Program. *Comput. Phys. Commun.* **1980**, *19* (2), 215−261.
(35) Stipa, P.; Marano, S.; Galeazzi, R.; Minnelli, C.; Laudadio, E. Molecular Dynamics Simulations of Quinine Encapsulation into Biodegradable Nanoparticles: A Possible New Strategy against Sars-CoV-2. *Eur. Polym. J.* **2021**, *158*, 110685.
(36) Laudadio, E.; Galeazzi, R.; Mobbili, G.; Minnelli, C.; Barbon, A.; Bortolus, M.; Stipa, P. Depth Distribution of Spin-Labeled Liponitroxides within Lipid Bilayers: A Combined EPR and Molecular Dynamics Approach. *ACS Omega* **2019**, *4* (3), 5029−5037.
(37) Zhang, R.; Gao, C.; Pan, S.; Shang, R. Fusion of GNSS and Speedometer Based on VMD and Its Application in Bridge Deformation Monitoring. *Sensors* **2020**, *20* (3), 694.
(38) Pettersen, E. F.; Goddard, T. D.; Huang, C. C.; Couch, G. S.; Greenblatt, D. M.; Meng, E. C.; Ferrin, T. E. UCSF Chimera—A Visualization System for Exploratory Research and Analysis. *J. Comput. Chem.* **2004**, *25* (13), 1605−1612.
(39) Spitalsky, Z.; Tasis, D.; Papagelis, K.; Galiotis, C. Carbon Nanotube−Polymer Composites: Chemistry, Processing, Mechanical and Electrical Properties. *Prog. Polym. Sci.* **2010**, *35* (3), 357−401.
(40) Lizundia, E.; Oleaga, A.; Salazar, A.; Sarasua, J. R. Nano- and Microstructural Effects on Thermal Properties of Poly (l-Lactide)/Multi-Wall Carbon Nanotube Composites. *Polymer* **2012**, *53*, 2412−2421.
(41) Kuang, T.; Chang, L.; Chen, F.; Sheng, Y.; Fu, D.; Peng, X. Facile Preparation of Lightweight High-Strength Biodegradable Polymer/Multi-Walled Carbon Nanotubes Nanocomposite Foams for Electromagnetic Interference Shielding. *Carbon* **2016**, *105*, 305−313.
(42) Hamedi, M. M.; Hajian, A.; Fall, A. B.; Hkansson, K.; Salajkova, M.; Lundell, F.; Wgberg, L.; Berglund, L. A. Highly Conducting, Strong Nanocomposites Based on Nanocellulose-Assisted Aqueous Dispersions of Single-Wall Carbon Nanotubes. *ACS Nano* **2014**, *8* (3), 2467−2476.
(43) Sandler, J. K. W.; Kirk, J. E.; Kinloch, I. A.; Shaffer, M. S. P.; Windle, A. H. Ultra-Low Electrical Percolation Threshold in Carbon-Nanotube-Epoxy Composites. *Polymer* **2003**, *44* (19), 5893−5899.
(44) Bauhofer, W.; Kovacs, J. Z. A Review and Analysis of Electrical Percolation in Carbon Nanotube Polymer Composites. *Compos. Sci. Technol.* **2009**, *69* (10), 1486−1498.
(45) Nguyen, T. D.; Sierra, E.; Eguiraun, H.; Lizundia, E. Iridescent cellulose nanocrystal films: the link between structural colour and Bragg's law. *Eur. J. Phys.* **2018**, *39*, No. 045803.
(46) Walters, M. C.; Matharu, G. K.; Hamad, W. Y.; Lizundia, E.; MacLachlan, M. J. Chiral Nematic Cellulose Nanocrystal/Germania and Carbon/Germania Composite Aerogels as Supercapacitor Materials. *Chem. Mater.* **2021**, *33* (13), 5197−5209.
(47) Lizundia, E.; Sarasua, J. R.; D'Angelo, F.; Orlacchio, A.; Martino, S.; Kenny, J. M.; Armentano, I. Biocompatible Poly(L-Lactide)/MWCNT Nanocomposites: Morphological Characterization, Electrical Properties, and Stem Cell Interaction. *Macromol. Biosci.* **2012**, *12* (7), 870−881.
(48) Xu, J.; Nguyen, T.-D.; Xie, K.; Hamad, W. Y.; MacLachlan, M. J. Chiral Nematic Porous Germania and Germanium/Carbon Films. *Nanoscale* **2015**, *7* (31), 13215−13223.
(49) Lizundia, E.; Nguyen, T.-D.; Vilas, J. L.; Hamad, W. Y.; MacLachlan, M. J. Chiroptical Luminescent Nanostructured Cellulose Films. *Mater. Chem. Front* **2017**, *1* (5), 979−987.
(50) Giese, M.; Spengler, M. Cellulose Nanocrystals in Nano-architectonics − towards Photonic Functional Materials. *Mol. Syst. Des. Eng.* **2019**, *4* (1), 29−48.
(51) Liu, D.; Dong, Y.; Liu, Y.; Ma, N.; Sui, G. Cellulose Nanowhisker (CNW)/Graphene Nanoplatelet (GN) Composite Films With Simultaneously Enhanced Thermal, Electrical and Mechanical Properties. *Front. Mater.* **2019**, *6*, 235.
(52) Xin, F.; Li, L. Decoration of Carbon Nanotubes with Silver Nanoparticles for Advanced CNT/Polymer Nanocomposites. *Compos. Part Appl. Sci. Manuf.* **2011**, *42* (8), 961−967.
(53) Dhamodharan, D.; Dhinakaran, V.; Ghoderao, P. NP.; Byun, H.-S.; Wu, L. Synergistic Effect of Cellulose Nanocrystals-Graphene Oxide as an Effective Nanofiller for Enhancing Properties of Solventless Polymer Nanocomposites. *Composites, Part B* **2022**, *238*, 109918.
(54) Oh, S. Y.; Yoo, D. I.; Shin, Y.; Seo, G. FTIR Analysis of Cellulose Treated with Sodium Hydroxide and Carbon Dioxide. *Carbohydr. Res.* **2005**, *340* (3), 417−428.
(55) Fortunati, E.; Mattioli, S.; Armentano, I.; Kenny, J. M. Spin Coated Cellulose Nanocrystal/Silver Nanoparticle Films. *Carbohydr. Polym.* **2014**, *113*, 394−402.
(56) Kamal, T.; Ahmad, I.; Khan, S. B.; Asiri, A. M. Synthesis and Catalytic Properties of Silver Nanoparticles Supported on Porous Cellulose Acetate Sheets and Wet-Spun Fibers. *Carbohydr. Polym.* **2017**, *157*, 294−302.
(57) Hamad, W. Y.; Hu, T. Q. Structure-Process-Yield Interrelations in Nanocrystalline Cellulose Extraction. *Can. J. Chem. Eng.* **2010**, *88* (3), 392−402.
(58) Lin, N.; Bruzzese, C.; Dufresne, A. TEMPO-Oxidized Nanocellulose Participating as Crosslinking Aid for Alginate-Based Sponges. *ACS Appl. Mater. Interfaces* **2012**, *4* (9), 4948−4959.
(59) Fallah-Shojaei, A.; Tabatabaeian, K.; Shirini, F.; Hejazi, S. Z. Multi-Walled Carbon Nanotube Supported Fe3O4NPs: An Efficient

https://doi.org/10.1021/acs.jpcc.3c04767
J. Phys. Chem. C XXXX, XXX, XXX−XXX

and Reusable Catalyst for the One-Pot Synthesis of 4H-Pyran Derivatives. *RSC Adv.* **2014**, *4* (19), 9509−9516.
(60) Tamilarasan, P.; Ramaprabhu, S. Ionic Liquid-Functionalized Partially Exfoliated Multiwalled Carbon Nanotubes for High-Performance Supercapacitors. *J. Mater. Chem. A* **2014**, *2* (34), 14054−14063.
(61) Sabzi, M.; Mersagh Dezfuli, S. A Study on the Effect of Compositing Silver Oxide Nanoparticles by Carbon on the electrochemical Behavior and Electronic Properties of Zinc-Silver Oxide Batteries. *Int. J. Appl. Ceram. Technol.* **2018**, *15* (6), 1446−1458.
(62) Fortunati, E.; D'Angelo, F.; Martino, S.; Orlacchio, A.; Kenny, J. M.; Armentano, I. Carbon Nanotubes and Silver Nanoparticles for Multifunctional Conductive Biopolymer Composites. *Carbon* **2011**, *49* (7), 2370−2379.
(63) Migahed, M. D.; Ishra, M.; Fahmy, T.; Barakat, A. Electric Modulus and AC Conductivity Studies in Conducting PPy Composite Films at Low Temperature. *J. Phys. Chem. Solids* **2004**, *65* (6), 1121−1125.
(64) Belattar, J.; Graça, M. P. F.; Costa, L. C.; Achour, M. E.; Brosseau, C. Electric Modulus-Based Analysis of the Dielectric Relaxation in Carbon Black Loaded Polymer Composites. *J. Appl. Phys.* **2010**, *107* (12), 124111.
(65) Zhu, C.; Monti, S.; Mathew, A. P. Evaluation of Nanocellulose Interaction with Water Pollutants Using Nanocellulose Colloidal Probes and Molecular Dynamic Simulations. *Carbohydr. Polym.* **2020**, *229*, 115510.
(66) Etale, A.; Onyianta, A. J.; Turner, S. R.; Eichhorn, S. J. Cellulose: A Review of Water Interactions, Applications in Composites, and Water Treatment. *Chem. Rev.* **2023**, *123*, 2016−2048.
(67) Alqus, R.; Eichhorn, S. J.; Bryce, R. A. Molecular Dynamics of Cellulose Amphiphilicity at the Graphene−Water Interface. *Biomacromolecules* **2015**, *16*, 1771−1783, DOI: 10.1021/acs.biomac.5b00307.
(68) Kulasinski, K.; Guyer, R.; Derome, D.; Carmeliet, J. Water Adsorption in Wood Microfibril-Hemicellulose System: Role of the Crystalline−Amorphous Interface. *Biomacromolecules* **2015**, *16* (9), 2972−2978.

https://doi.org/10.1021/acs.jpcc.3c04767
J. Phys. Chem. C XXXX, XXX, XXX−XXX